Supporting Information

Cu and Fe dual-atom nanozyme mimicking cytochrome c oxidase to boost the oxygen reduction reaction

Cheng Du,[a, d, †] Yijing Gao,[b, †] Hengquan Chen,[c] Ping Li,[a, d] Shuyun Zhu,[e] Jianguo Wang,*[b] Qinggang He,*[c] and Wei Chen*[a, d]

[a] State Key Laboratory of Electroanalytical Chemistry, Changchun Institute of Applied Chemistry, Chinese Academy of Sciences, Changchun, Jilin 130022, China

[b] Institute of Industrial Catalysis, State Key Laboratory Breeding Base of Green-Chemical Synthesis Technology, College of Chemical Engineering, Zhejiang University of Technology, Hangzhou 310032, P.R. China

[c] College of Chemical and Biological Engineering, Zhejiang University, Hangzhou, Zhejiang 310027, China

[d] University of Science and Technology of China, Hefei, Anhui 230029, P.R.China

[e]School of Chemistry and Chemical Engineering, Qufu Normal University, Qufu, Shandong, China

* Corresponding author. E-mail: weichen@ciac.ac.cn; jgw@zjut.edu.cn; qghe@zju.edu.cn

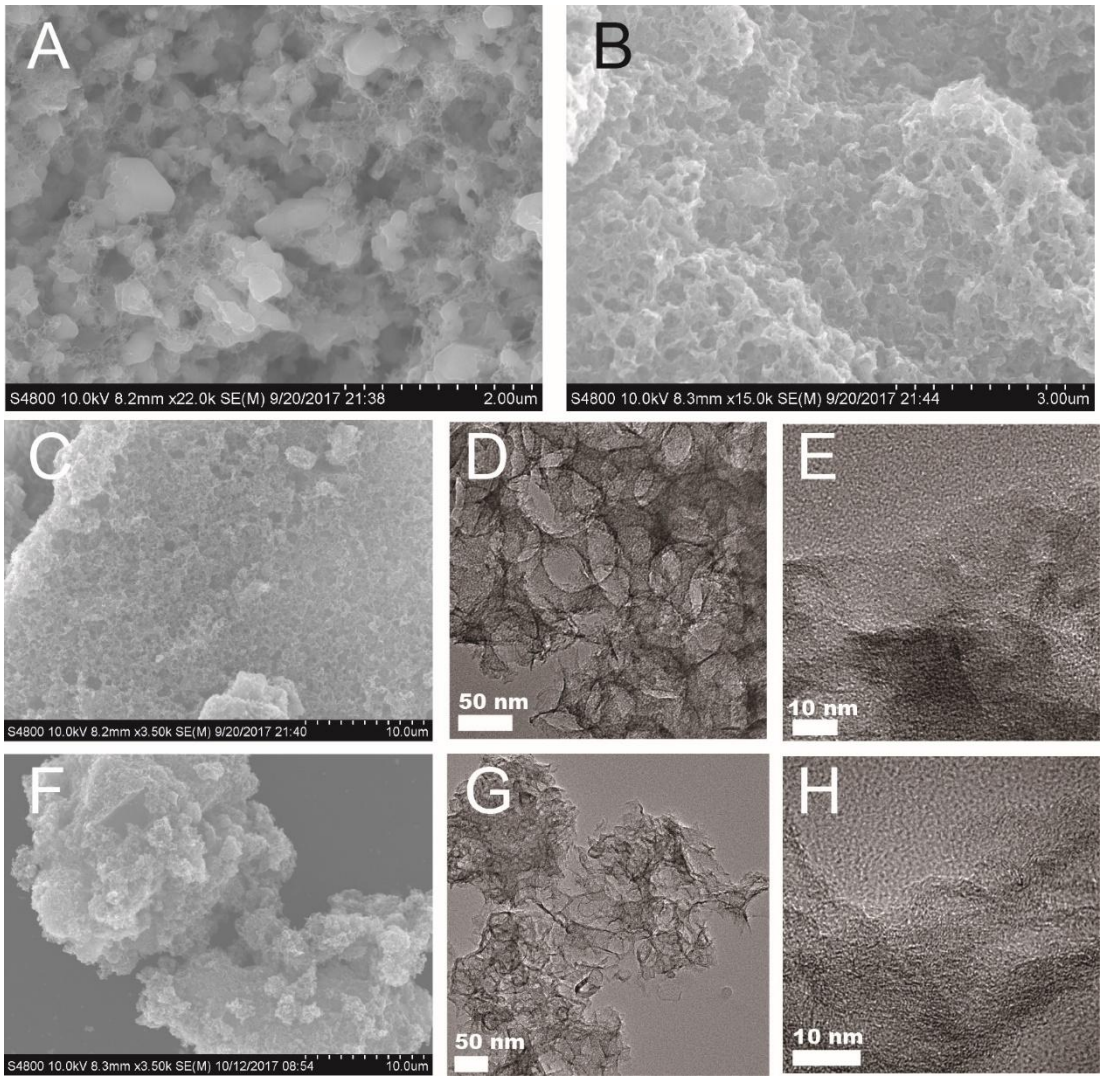

Fig. S1 (A-B) SEM images of FeCu-DA/NC before (A) and after (B) the acid washing step; SEM (C) and TEM (D-E) images of Fe-SA/NC; SEM (F) and TEM (G-H) images of Cu-SA/NC.

After the calcination step, large CaO nanoparticles are obviously observed in Fig. S1A. After acid washing, the CaO nanoparticles derived from nano-$CaCO_3$ have been completely removed and macroporous 3D structure can be formed, as observed from Fig. S1B. Similar to the FeCu-DA/NC, the Fe-SA/NC and Cu-SA/NC still keep the 3D porous structures (Fig. S1C and Fig. S1F). Additionally, there is no nanoparticle in the HRTEM images (Fig. S1D, S1E, S1G and S1H), indicating the atomic dispersions of Fe and Cu in the Fe-SA/NC, Fe-SA/NC and Cu-SA/NC samples.

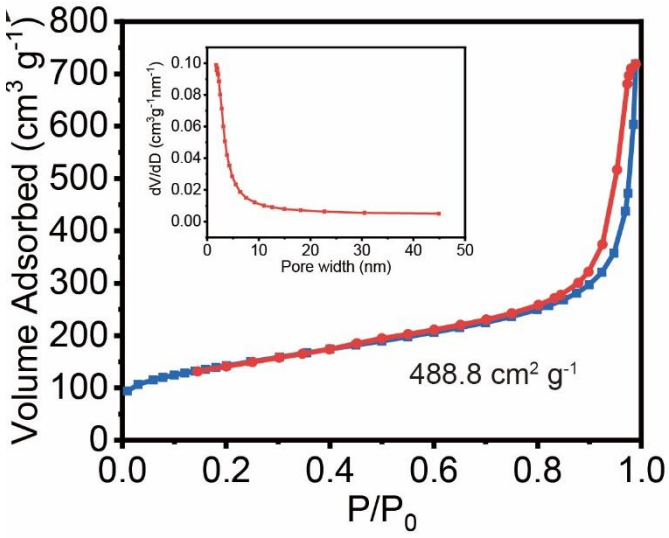

Fig. S2 Nitrogen adsorption-desorption isotherm of FeCu-DA/NC; the inset is the pore size distribution plot.

The BET specific surface area of FeCu-DA/NC is calculated to be as large as 488.8 cm^2 g^{-1} (Figure S2A), which is beneficial for the exposure of active sites.

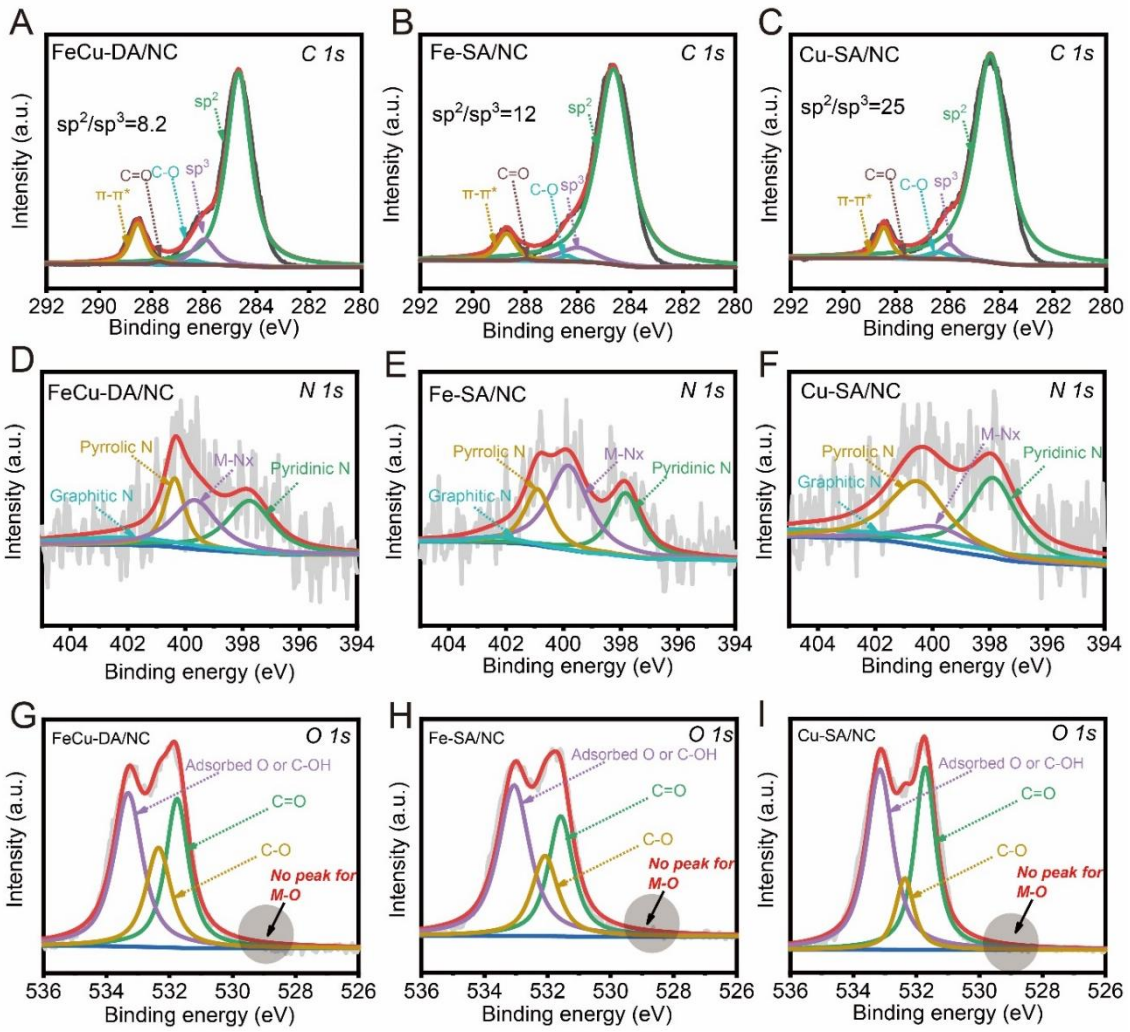

Fig. S3 C1s XPS spectra of FeCu-DA/NC (A), Fe-SA/NC (B) and Cu-SA/NC (C); N1s XPS spectra of FeCu-DA/NC (D), Fe-SA/NC (E) and Cu-SA/NC (F); O1s XPS spectra of FeCu-DA/NC (G), Fe-SA/NC (H) and Cu-SA/NC (I).

As seen in Fig. S3A-C, the C1s spectra can be deconvoluted into five peaks, i.e. sp^2 (284.6 eV), sp^3 (285.98 eV), C-O (286.4 eV), C=O (287.7 eV) and π-π* (289.5 eV). The sp^2 and sp^3 refer to the basal-plane and defect of carbon atoms, respectively. Thus, the defect level of carbon materials is reflected by the sp^3 content. Compared to the Fe-SA/NC and Cu-SA/NC, the value of sp^2/sp^3 from the FeCu-DA/NC decreases from 25 and 12 to 8.2, suggesting more defects in FeCu-DA/NC, which is in agreement with the result of Raman spectra. As seen in Fig. S3D-F, the N1s spectra can be deconvoluted into four peaks, pyridinic N (397.7 eV), M-N (399.8 eV), pyrrolic N (400.9 eV), and graphitic N (402.3 eV), respectively. As shown in Fig. S3G-I, the O1s spectra can be deconvoluted into three peaks, i.e. C=O (531.7 eV), C-O (532.4 eV) and adsorbed O or C-OH (533.2 eV), respectively. The existence of M-N and absence of M-O bond prove the $M\text{-}N_4$ fitting results in XAFS.

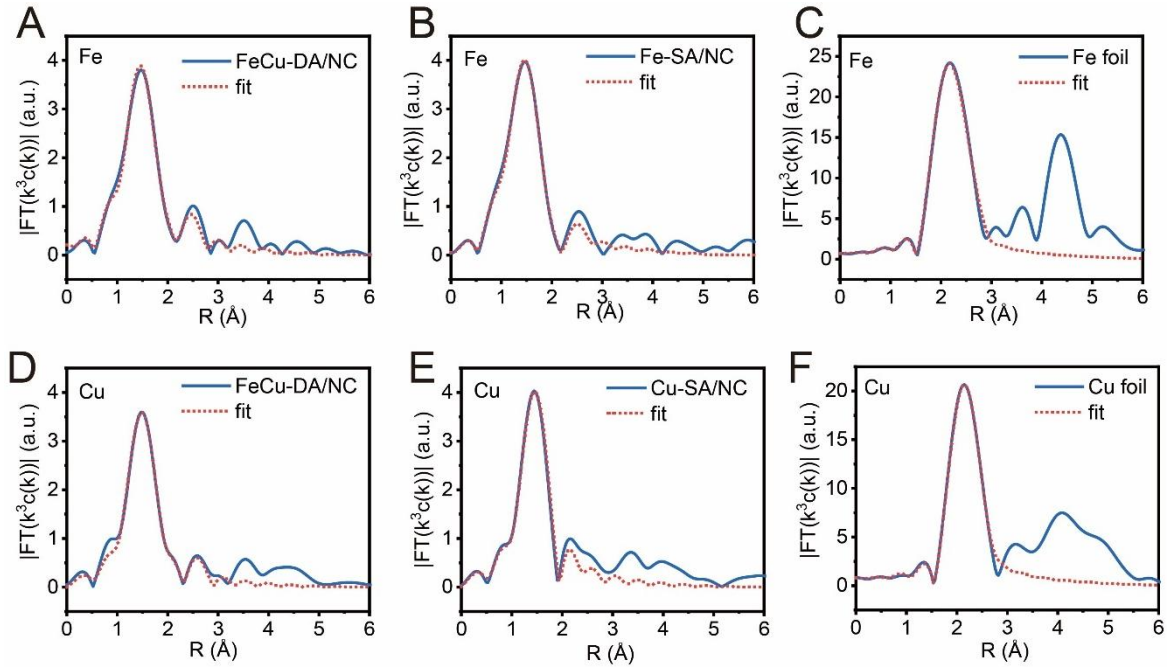

Fig. S4 (A-C) Fe K-edge Fourier-transform EXAFS in R space and the corresponding EXAFS fitting curves of FeCu-DA/NC (A), Fe-SA/NC (B) and Fe foil (C); (D-F) Cu K-edge Fourier-transform EXAFS in R space and the corresponding EXAFS fitting curves of FeCu-DA/NC (D), Cu-SA/NC (E) and Cu foil (F).

Table S1 EXAFS fitting results of the three samples

Sample	**shell**	**N**	**R/Å**	**$\Delta\sigma^2$*1000/Å^2**	**ΔE_0/eV**
Cu-SA/NC	Cu-N	3.9	1.94	7.3	-7.56
	Cu-C	8.0	2.70	4.3	1.00
Fe-SA/NC	Fe-N	3.8	2.01	11.6	-3.06
	Fe-C	8.0	2.92	11.9	-10.00[set]
FeCu-DA/NC	Cu-N	4.0	1.97	9.5	-4.61
	Cu-C	8.0	2.80	13.3	-5.89
	Fe-N	4.0	2.00	8.2	-3.43
	Fe-C	8.0	3.13	10.5	-4.11

N: coordination number; R: bond length; σ^2: the Debye-Waller factor to account for both thermal and structural disorders; ΔE_0: E_0 shift.

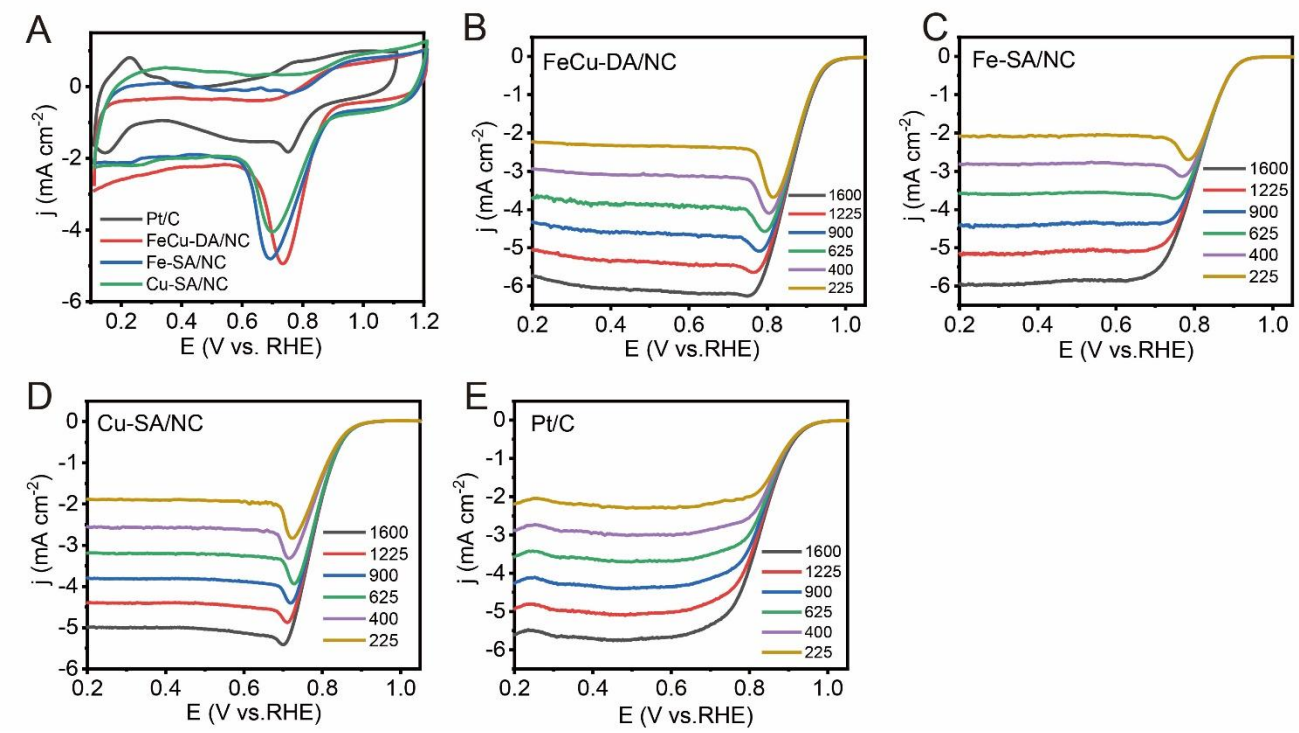

Fig. S5 CV curves (A) and LSV curves under different rotational speeds of FeCu-DA/NC (B), Fe-SA/NC (C), Cu-SA/NC (D) and Pt/C (E) in O2-saturated 0.1 M KOH with a scan rate of 100 mV/s for CV and 5 mV/s for LSV.

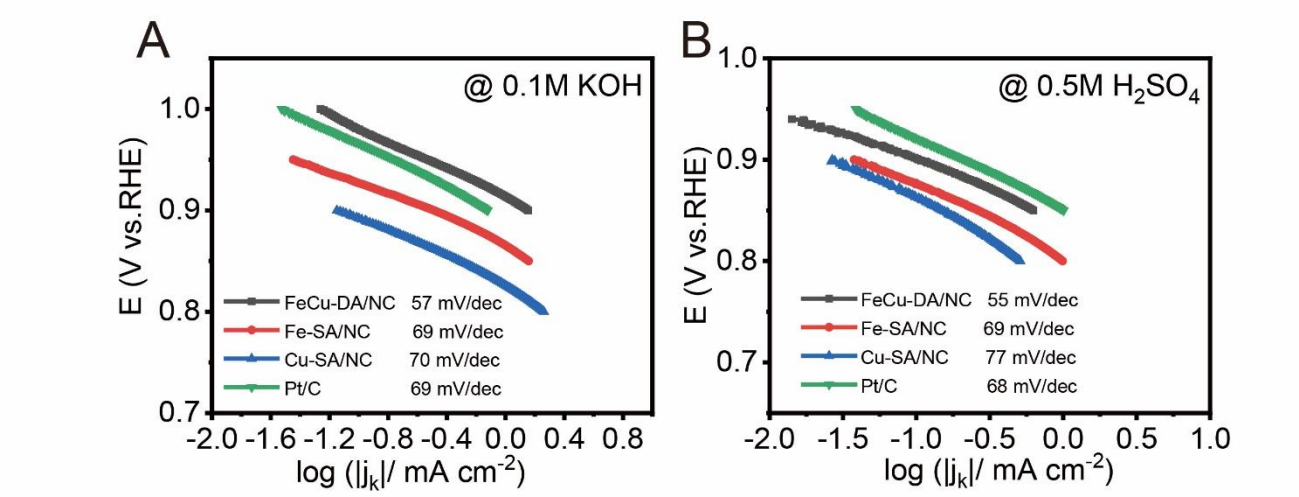

Fig. S6 Tafel plots of ORR on the prepared samples in 0.1 M KOH (A) and 0.5 M H_2SO_4 (B).

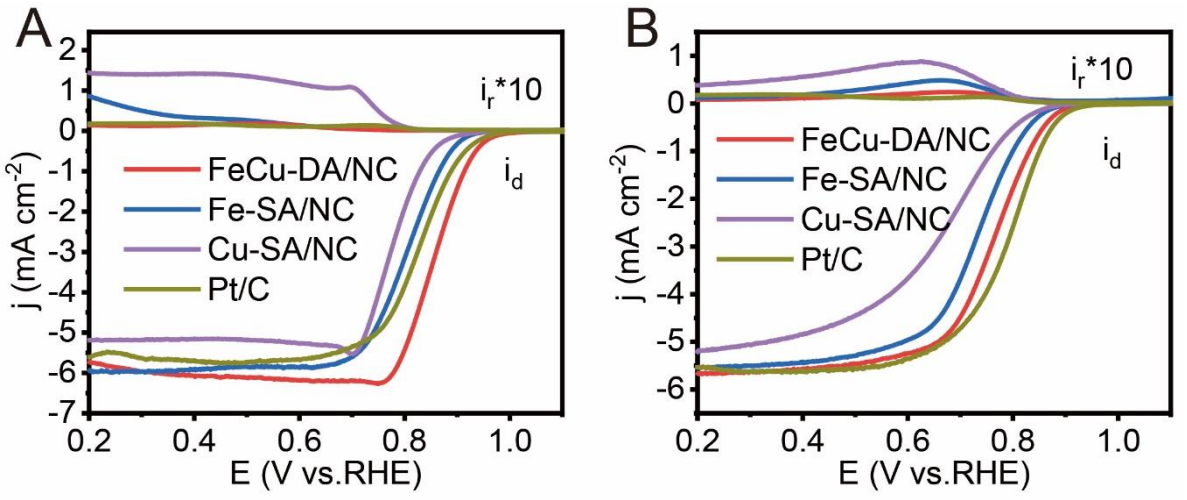

Fig. S7 RRDE curves of the samples in O_2-saturated 0.1 M KOH (A) and 0.5 M H_2SO_4 (B) with a scan rate of 5 mV s^{-1} under 1600 rpm.

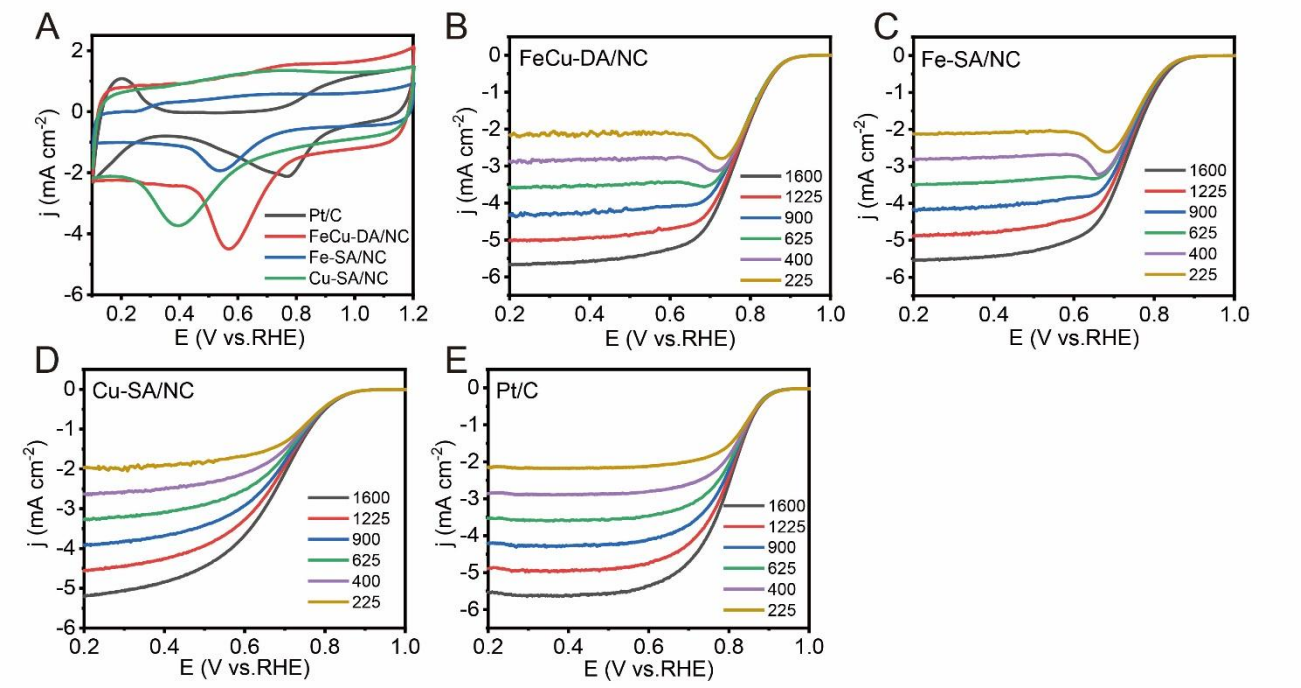

Fig. S8 (A) CV curves on the studied catalysts in O_2-saturated 0.5 M H_2SO_4 with a scan rate of 100 mV s^{-1}. (B-E) LSV curves under different rotational speeds on FeCu-DA/NC (B), Fe-SA/NC (C), Cu-SA/NC (D) and Pt/C (E) in O_2-saturated 0.5 M H_2SO_4 with a scan rate of 5 mV s^{-1}.

Table S2 Summary of recently reported ORR performances of single-atom catalysts

Materials	Electrolyte	$\Delta E_{1/2}$ (Vs. Pt/C)	Reference
Alkalic performance			
FeCu-DA/NC	**0.1M KOH**	**30 mV**	**This work**
Fe-SA/NC	0.1M KOH	-30 mV	This work
Cu-SA/NC	0.1M KOH	-50 mV	This work
CoNi-SAs/NC	0.1M KOH	-60 mV	Adv. Mater. 2019, 1905622
Fe_2–N–C	0.1M KOH	+40 mV	Chem 2019, 5, 2865-2878
Fe/OES	0.1M KOH	0 mV	Angew Chem Int Ed 2020, 59, 7384-7389
Cu-SAs/N-G	0.1M KOH	+25 mV	Nature Catalysis 2018,1, 781–786
AC@f-FeCoNC900	0.1M KOH	+50 mV	Energy Environ. Sci., 2019,12, 1317-1325
Cu−N_4–C	0.1M KOH	-20 mV	ACS Nano 2019, 13, 3, 3177–3187
Fe–N–C HNSs	0.1M KOH	+30 mV	Adv. Mater. 2018, 1806312
SC-Fe	0.1M KOH	~0 mV	Angew. Chem. Int. Ed. 2019, 58, 1 – 6
SA-Fe/NG	0.1M KOH	+30 mV	PNAS, 2018, 115, 6626-6631
Acidic performance			
FeCu-DA/NC	**0.5M H_2SO_4**	**-20 mV**	**This work**
Fe-SA/NC	0.5M H_2SO_4	-60 mV	This work
Cu-SA/NC	0.5M H_2SO_4	-110 mV	This work
Fe(Zn)-N-C	0.1 M HClO4	-40 mV	Angew. Chem. Int. Ed. 10.1002/anie.202004534
TPI@Z8(SiO_2)-650-C	0.5M H_2SO_4	-12 mV	Nature Catal. 2019, 2, 259-268
Fe−N_4-C-80	0.1 M HClO4	-40 mV	Adv Mater 2020, 32, 2000966
Fe_2–N–C	0.5M H_2SO_4	-20 mV	Chem 2019, 5, 2865-2878
Fe/OES	0.5M H_2SO_4	-15 mV	Angew Chem. Int. Ed. 2020, 59, 7384-7389
H-Fe-N_x-C	0.5M H_2SO_4	-50 mV	ACS Nano 2019, 13, 7, 8087−8098
Cu-SAs/N-G	0.1 M HClO4	>-100 mV	Nature Catal. 2018,1, 781–786
20Co-NC-1100	0.5M H_2SO_4	-60 mV	Adv. Mater. 2018, 1706758
p-Fe-N-CNFs	0.1 M HClO4	-100 mV	Energy Environ. Sci., 2018, 11(8): 2208-2215.

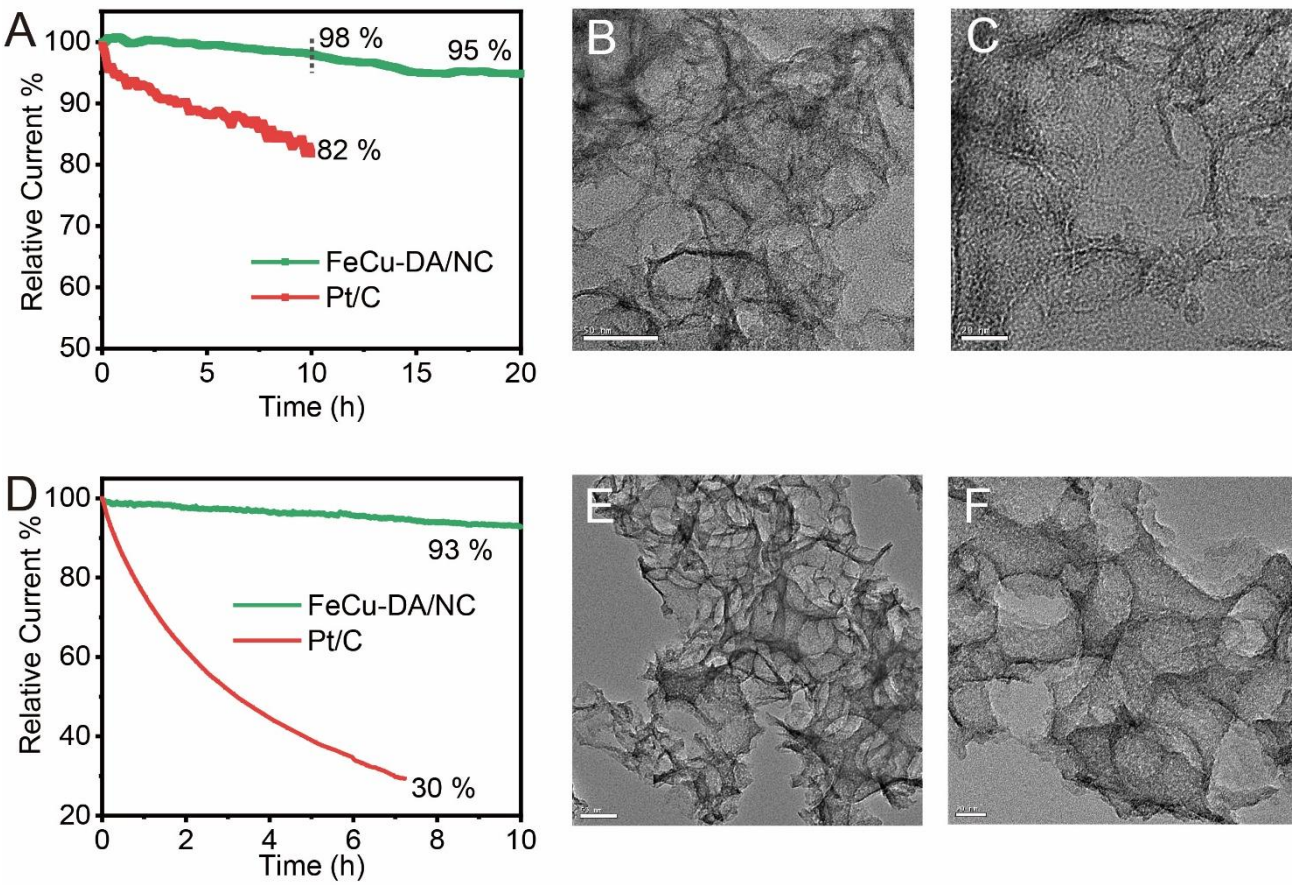

Fig. S9 (A) The ADT results of FeCu-DA/NC and Pt/C in O_2-saturated 0.1 M KOH under 1600 rpm at 0.4 V; (B-C) TEM images of FeCu-DA/NC after ADTs in 0.1 M KOH; (D) The ADT results of FeCu-DA/NC and Pt/C in O_2-saturated 0.5 M H_2SO_4 under 1600 rpm at 0.4 V; (E-F) TEM images of FeCu-DA/NC after ADTs in 0.5 M H_2SO_4.

After 20 hours of ADTs in 0.1 M KOH, 95% of the ORR current can be maintained on FeCu-DA/NC (Fig. S9A). However, only 82% of the original current is kept on Pt/C after only 10 hours of ADTs. In the acid medium, the FeCu-DA/NC remains 93% of the ORR current after 10 hours of ADTs (Fig. S9D). However, only 30% of the original current remains on the Pt/C after only 7 hours of ADTs. Additionally, there is no obvious morphology change in the TEM images after ADTs in both acid and base conditions (Fig. S10B-C and E-F). In particular, no nanoparticles can be found in the TEM images, demonstrating the high stability of the atomically dispersed Fe and Cu. For Pt/C, the interaction between Pt nanoparticles and carbon support is just from the weak physical adsorption. However, the metal atoms in the single-atom catalysts are supported on the carbon support through strong covalent bonds. Therefore, the single-atom catalyst shows much higher stability than the commercial Pt/C catalysts.

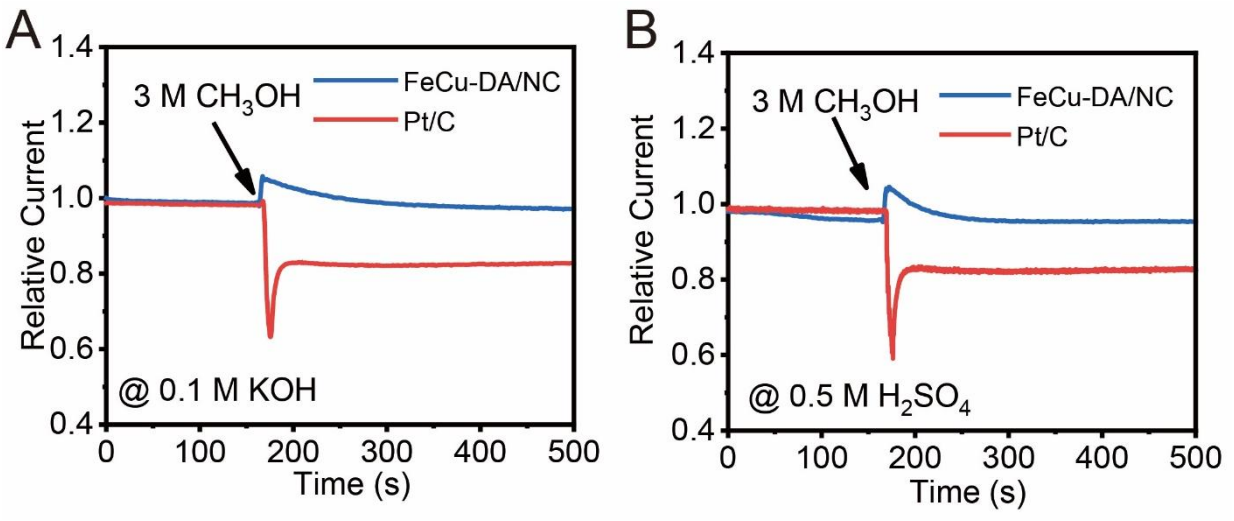

Fig. S10 The methanol crossover tests of FeCu-DA/NC and Pt/C in O_2-saturated 0.1 M KOH (A) and 0.5 M H_2SO_4 (B) under 1600 rpm at 0.4 V.

The ORR current from FeCu-DA/NC can be almost fully recovered after the short abrupt jump caused by the addition of 3 M CH_3OH in both acid and base. However, the Pt/C exhibits serious poisoning with large current decrease. Such results confirm that the FeCu-DA/NC owns remarkably better anti-poisoning ability than Pt/C in both base and acid media.